Exploiting Channel Diversity in Secret Key Generation from Multipath Fading Randomness

Yanpei Liu, *Student Member, IEEE,* Stark C. Draper, *Member, IEEE,* Akbar M. Sayeed, *Fellow, IEEE*

arXiv:1107.3534v2 [cs.CR] 1 Jul 2012

***Abstract*—We design and analyze a method to extract secret keys from the randomness inherent to wireless channels. We study a channel model for multipath wireless channel and exploit the channel diversity in generating secret key bits. We compare the key extraction methods based both on entire channel state information (CSI) and on single channel parameter such as the received signal strength indicators (RSSI). Due to the reduction in the degree-of-freedom when going from CSI to RSSI, the rate of key extraction based on CSI is far higher than that based on RSSI. This suggests that exploiting channel diversity and making CSI information available to higher layers would greatly benefit the secret key generation. We propose a key generation system based on low-density parity-check (LDPC) codes and describe the design and performance of two systems: one based on binary LDPC codes and the other (useful at higher signal-to-noise ratios) based on four-ary LDPC codes.**

***Index Terms*—Common randomness, secret key generation, channel diversity, LDPC codes, Slepian-Wolf decoder**

I. Introduction

In this paper we study the generation of secret keys based on the inherent randomness of wireless multipath channels. This study falls into the broad area of physical layer security (see [1] for an overview of the area). In this setting the objective is for a pair of users, generically referred to as *Alice* and *Bob*, to extract a secret key from a naturally occurring source of randomness observed by two users. The central idea is that through a public (i.e., *not* secret) discussion, Alice and Bob can de-noise their correlated observations to generate, with high probability, a commonly known string, which can serve as the key. Of course, any eavesdropper (typically named *Eve*) would use both her knowledge of the public message and any observation she has to guess the key. A source of naturally occurring randomness that would be well suited to the key generation application would be characterized by three properties. It would be easily and widely accessible, it would have a high level of randomness, and it would be difficult for Eve to observe. The randomness inherent to wireless multipath fading channels, such as the random amplitudes and phases of the channel response coefficients, satisfies all three properties.

Copyright (c) 2012 IEEE. Personal use of this material is permitted. However, permission to use this material for any other purposes must be obtained from the IEEE by sending a request to pubs-permissions@ieee.org.

This work was presented in part at the 45th annual Conference on Information Sciences and Systems (CISS), Baltimore MD, March 2011.

The authors are with the Dept. of Electrical and Computer Engineering, University of Wisconsin, Madison, WI 53706 (E-mail: {yliu73@wisc.edu, sdraper@ece.wisc.edu, akbar@engr.wisc.edu}).

Y. Liu and S. C. Draper were supported by the National Science Foundation under grant CCF-0963834 and by a grant from the Wisconsin Alumni Research Foundation.

The ubiquity of personal wireless devices makes a multipath fading channel an easily accessible, and hence very relevant, source of randomness. The fact that it has a high level of randomness and is difficult to eavesdrop is due to the physics of electromagnetic wave propagation. In a rich multipath environment wireless channels have high spatial and temporal variation. For instance, whenever either Alice or Bob moves, or whenever other scattering objects move between them, the channel between them changes. In terms of key extraction this means that there is a continual influx of new randomness from which to extract new and independent key bits. For the same reason, an eavesdropper that is listening on transmission between Alice and Bob and that is even a few wavelengths away from either will observe a nearly independent channel. In terms of key extraction, this makes it difficult to eavesdrop on the source of randomness (the channel coefficients).

Modern wireless communication protocols typically use diversity signaling techniques such as orthogonal frequency-division multiplexing (OFDM) or Multiple Input Multiple Output (MIMO) antennas. These techniques exploit frequency, time and spatial diversity of the underlying wireless channel and improve the communication performance. By exploiting channel diversity in a similar manner in secret key generation one can harvest more randomness. Thus in this paper, we study an OFDM system as an example from the perspective of secret key generation. We characterize the suitableness of such channels for key generation, both under the assumption of the availability of full channel state information (CSI) and the assumption of the availability of only received signal strength indicators (RSSI). The latter is what is available to the higher layers of existing wireless transceivers. We show that by exploiting the channel diversity in the CSI, one can significantly increase the rate at which the secret key bits can be generated relative to when channel diversity is not exploited (such as RSSI based method). Thus making CSI available to the higher layers (where security is managed) in future transceiver designs would greatly facilitate the adoption of the approach we propose. We also show that when extracting keys from CSI, one can, without loss of rate, extracts key bits separately from the real and the imaginary parts of each channel coefficient. The same is not true for amplitude and phase as there is correlation between the amplitudes and phases *across* two participating users. We also detail an algorithm of the de-noising needed in key extracted. Our algorithm is based on low-density parity-check (LDPC) codes. We describe two designs. One based on binary and one based on non-binary (quaternary) LDPC codes. Higher-alphabet codes are required to extract the full randomness of the channel at higher signal-

to-noise ratios (SNR).

There are many works in both theoretical analysis and practical implementation of physical layer security. Theoretical analysis in wire-tap channel date back to four decades ago [2], [3] More recently, Bloch et al. propose the seminal practical opportunistic one-way secret key agreement protocol for Gaussian wiretap channel in [4]. The works done by Maurer [5] and Ahlswede and Csiszár [6] show that correlated randomness can be used to generate secret keys. Their works lay down the analytical foundations for secret key generation in wireless communication. Sayeed and Perrig [7] recognize the possibility of extracting secret keys from multipath randomness in wireless communication. Fundamental limits to key generation for multipath randomness are studied in [8]–[13]. In [8], [9] the minimum energy-per-key-bit is characterized for rich fading channels and is extended in [14] to sparse multipath channels. Eavesdropper with the ability to tamper the transmission has been studied by Maurer and Wolf [15]–[17]. More recently, Chou et al. study the secret key capacity of the sender-excited secret key agreement in [18]. Non-coherent secret key generation in which neither the sender nor the receiver have access to the channel state information has been studied in [19].

There are also many works on realizing physical layer security by designing practical secret key generating systems. These works are based on the earliest work by Hershey et al. [20] and Hassan et al. [21]. Ye et al. [22], [23] present an over-the-air implementation on 802.11 platforms, prototyping a systematic design using a scalar fading channel coefficient. Jana et al. present yet another over-the-air implementation using the received signal strength indicators [24]. Channel randomness is also exploited for device pairing [25] and authentication [26]–[28]. Secret key generation system over MIMO has been considered in [29] and the references therein.

There are many related design related issues. Typical secret key generation process consists of three phases: randomness exploration, reconciliation and privacy amplification [23]. In randomness exploration, quantization is used to convert continuous observations to discretized information bits. A good quantizer should not only maximize the mutual information between Alice and Bob's bit sequences, but also reveal limited information to the eavesdropper. An algorithm is proposed in [30], [31] to find such a quantizer. Ye et al. [23] propose an over-quantization technique to extract more bits per independent channel training. When the channel is over-static (long coherence time), filtering techniques, such as Discrete Cosine Transform in [32] and windowed moving average low pass filtering in [23], are used to remove the redundancy in the extracted key bits. Reconciliation process is typically done using various coding techniques, such as LDPC codes [4] and list-encoding [25]. For a detailed survey on reconciling two binary random variables, see [33]. Finally, universal hash functions are widely used [17], [34] for privacy amplification.

In this paper, we show that the channel randomness can be further exploited through the channel diversity offered by the wireless front-end. We note that in many related works, such as [22]–[25], secret key bits are extracted from a single parameter observed in wireless channel. This fundamentally limits the rate at which the secret key bits that can be extracted. For instance, in [22] only one bit can be extracted per independent channel realization although they over-quantize it to increase the number of bits in their later work [23]. Similarly, in [25] only one bit can be extracted per coherence time. We thus argue that by exploiting the channel diversity in wireless multipath fading channel, one can significantly improve the secret key capacity.

A. System overview

To lend concreteness to the ensuing discussion we describe the operation of the key extraction algorithm discussed later in the paper. To generate their correlated observations Alice and Bob each transmits known channel sounding (training) signals to each other. This two-way training is done in two consecutive time slots. As long as the channel is static over these two time slots (the key assumption of our model [7], [24]) then, due to the reciprocity of electromagnetic wave propagation, Alice and Bob both obtain (noisy) observations of the same multipath fading channel coefficients. Eve is assumed to listen to both transmissions, but due to the fast spatial decorrelation of multipath channels, we assume for the remainder of the paper that her observations are independent and thus useless for estimating the realized channel law. Alice then quantizes her observations into some finite alphabet. (If Alice did not quantize her observations there would be no way Bob could recover the *exact* same coefficients with high probability.) Alice then sends to Bob a public message. In our algorithm the public message is the syndrome of some length-N error correcting code where N is the length of Alice's vector of quantized channel coefficients. Bob combines the public message with his observations in his attempt to recover Alice's quantized observations. We describe two possibilities for Bob. First, that he quantizes his own observations before his recovery attempt ("hard" decoding) and, second, that he bases his recovery attempt on his un-quantized observations (strictly better "soft" decoding).

We do not consider authentication in our proposed secret key generation system [26]–[28]. Therefore, our system does not address active attacks such as man-in-the-middle attacks. One could always first authenticate the validity of Alice and Bob by using public key cryptography before invoking our secret key generation system.

B. Notation and outline

Unless otherwise specified, we use upper case letters, e.g., X to denote random variables and bold uppercase, e.g., $\mathbf{X}$ to denote random vectors; x and $\mathbf{x}$ are their respective realizations. If X is a complex random variable, we use $\Re(X)$ and $\Im(X)$ to denote, respectively, the real and imaginary parts of X. We use $X \sim \mathcal{CN}(m, \sigma^2)$ to denote a complex Gaussian random variable X with mean m, variance σ^2, and with real and imaginary parts independent and identically distributed.

The rest of the paper is organized as follows. In Sec. II we provide background material on the OFDM channel model. In Sec. III we define secret key capacity and introduce the measurement model. In Sec. IV we evaluate the secret key

capacity for various channels of interest, and draw a number of useful lessons for designs. In Sec. V we describe our designs and algorithms. In Sec. VI we provide numerical results for typical 802.11a parameter settings and secret key capacity. We conclude in Sec. VII. Some proofs are deferred to the Appendix.

II. Channel Diversity: An OFDM Example

In this section, we introduce diversity signaling technique used in OFDM system. We then characterize the channel coefficients which represent the channel diversity and from which we extract our secret keys. The OFDM model we use follows closely that introduced in [35].

A. OFDM signaling

Let T denote the signaling duration and W denote the two-sided bandwidth of a wireless link with $M = TW$. An OFDM system transmits M orthogonal signals. The transmitted signal $s(t)$ can be represented as

$$s(t) = \sum_{n=0}^{M-1} s_n \phi_n(t),\ 0 \le t \le T, \tag{1}$$

where the s_n are the information-bearing signal coefficients and the $\phi_n(t)$ are the orthogonal modulating waveforms or "tones". In OFDM the Fourier basis is used, i.e.,

$$\phi_n(t) = \begin{cases} \frac{1}{\sqrt{T}} e^{j2\pi n \Delta f t} & \text{if} \quad 0 \le t \le T \\ 0 & \text{else} \end{cases} \tag{2}$$

where $\Delta f = \frac{1}{T}$. The received signal $r(t)$ is $r(t) = h(t) * s(t) + w(t)$ where $h(t)$ is the communication channel, assumed to be time-invariant during the two-way training, $w(t)$ is the receiver noise, and $*$ denotes continuous-time convolution. We model $w(t)$ as a complex zero-mean white Gaussian noise process with autocorrelation function $E[w(t_1)w^*(t_2)] = \sigma_W^2 \delta(t_1 - t_2)$ where $\delta(\cdot)$ is the Dirac delta.

We discretize the observation $r(t)$ by projecting it onto the orthogonal basis functions $\phi_n(t)$ to produce

$$r_n = \int_{-\infty}^{\infty} r(t)\phi_n^*(t)dt = H_n s_n + w_n, \tag{3}$$

where

$$H_n = \int_{-\infty}^{\infty} \sqrt{T} h(t) \phi_n^*(t) dt$$

is the *frequency domain* channel coefficient at the n^{th} tone and the

$$w_n = \int_{-\infty}^{\infty} w(t)\phi_n^*(t)dt$$

are independent zero-mean complex Gaussian random variables of variance σ_W^2.

Wireless multipath channels $h(t)$ are well modeled in [35] as having an echo-type impulse response. In particular, let

$$h(t) = \sum_{k=1}^{N_p} \beta_k \delta(t - \tau_k) \tag{4}$$

where N_p is the total number of propagation paths, and $\tau_k \in [0, \tau_{\max}]$, $\tau_{\max}$ and β_k are the delay, the delay spread and the complex channel gain associated with the k^{th} path. Since τ_k is typically much longer than the speed of light divided by the carrier, each β_k is well modeled as having uniform random phase. Also, since the scaterring objects are distinct, β_k are well modeled as independent random variables. We incorporate an exponential power-delay profile where the variance of β_k decays with τ_k.

The frequency domain channel coefficients H_n, $0 \le n \le M-1$ are

$$H_n = \sum_{k=1}^{N_p} \beta_k e^{-j2\pi \frac{n}{T}\tau_k} \tag{5}$$

$$\approx \frac{1}{\sqrt{M}} \sum_{l=0}^{M-1} h_\ell e^{-j2\pi \frac{n\ell}{M}}, \tag{6}$$

where in (6) we approximate H_n by quantizing the τ_k into M delay bins and aggregating the effect of the β_k terms into the h_ℓ. Each bin is of length $\tau_{\text{bin}} = 1/W$ and

$$h_\ell = \sqrt{M} \sum_{k=1}^{N_p} \beta_k \text{sinc}\left[W\left(\frac{\ell}{W} - \tau_k\right)\right] \tag{7}$$

$$\approx \sqrt{M} \sum_{k:\, \frac{\ell-0.5}{W} < \tau_k \le \frac{\ell+0.5}{W}} \beta_k. \tag{8}$$

The variable h_ℓ is the *sampled* or *time domain* channel coefficient associated with the ℓ^{th} *resolvable* delay bin. If there are many β_k associated with each bin, as is the case for rich multipath, the h_ℓ are well approximated as zero-mean complex Gaussian random variables; a further approximation justified by the central limit theorem.

In OFDM channel, $\tau_{\max} \le T$, thus only the first few delay bins have physical paths contributing to them, similarly only the first few h_ℓ will be significant. Say the first $L \le M$ sampled channel coefficients are significant, then we further simplify our approximation of H_n as

$$H_n \approx \frac{1}{\sqrt{M}} \sum_{\ell=0}^{L-1} h_\ell e^{-j2\pi \frac{n\ell}{M}}. \tag{9}$$

where we have neglected the effect of the tails of the sinc waveforms in (7).

The h_ℓ is well modeled as having uniform phase (as remarked following (4)) and having a complex Gaussian distribution (as remarked following (8)). Since the paths aggregated into distinct h_ℓ are typically reflections from distinct scatters, the L non-zero h_ℓ are also often well modeled as being statistically independent. However, the h_ℓ are not identically distributed; the variance is roughly inversely proportional to τ_k as the result of the exponential power-delay profile on β_k. On the other hand, H_n exhibits Gaussian characteristic under rich multipath with variance σ_H^2. Following from (5), we have

$$\sigma_H^2 = E\left[|H_n|^2\right] = \sum_{k=1}^{N_p} E\left[|\beta_k|^2\right],$$

which does not depend on n. Hence, while the H_n are not independent, they have the same marginal distribution.

We note that if there are only a few transmission paths, the assumption that channel coefficients are Gaussian distributed

no longer holds. However, we are using Gaussian model as an example to illustrate the importance of exploiting channel diversity, which is actually not limited to Gaussian case.

B. Signal-to-noise ratio

As mentioned above, when multipath is rich, i.e., N_p is large, the H_n can be well modeled as $\mathcal{CN}(0, \sigma_H^2)$. We define the *per-tone* SNR as

$$SNR_f = \frac{E[H_n^2]}{E[w_n^2]} = \frac{\sigma_H^2}{\sigma_W^2}. \tag{10}$$

Also as discussed above, h_ℓ is well modeled as $\mathcal{CN}(0, \sigma_h^2(\ell))$. We can thus define the *time-domain* SNR as

$$SNR_\tau(\ell) = \frac{\sigma_h^2(\ell)}{\sigma_W^2}. \tag{11}$$

It can be shown that we have the relation

$$\sum_{\ell=0}^{L-1} SNR_\tau(\ell) \approx M \cdot SNR_f. \tag{12}$$

If the sampled channel coefficients have equal variance, the relationship simplifies to

$$SNR_\tau \approx \frac{M}{L} SNR_f. \tag{13}$$

III. Secret key systems: Definitions and measurement model

In this section we introduce the measurement model, secret key generation system, and study the secret key capacity.

A. System model

Secret key generation system has been studied by many authors. In particular, the authors in [5], [6] study the fundamental limits on the achievable secret key rates. We state their results for reference in the context of our application.

Definition 1. *A length-N secret key generation system over alphabets $\mathcal{X}_A, \mathcal{X}_B, \mathcal{K}, \mathcal{S}$ is a triplet of functions (f, g_A, g_B):*

$$f : \mathcal{X}_A^N \rightarrow \mathcal{K}^{NR}, \tag{14}$$

$$g_A : \mathcal{X}_A^N \rightarrow \mathcal{S}^m, \tag{15}$$

$$g_B : \mathcal{X}_B^N \times \mathcal{S}^m \rightarrow \mathcal{X}_A^N. \tag{16}$$

We interpret this definition in the context of the system operation described in Sec. I-A. The function f maps Alice's source of randomness into the secret key. The function g_A defines the public message Alice sends to Bob. The function g_B is Bob's decoding function that maps his observation and the public message into his estimate of Alice's observation. If Bob's estimate is correct applying $f(\cdot)$ to it will recover the key.

Given a source of randomness $p_{X_A^N, X_B^N}(x_A^N, x_B^N)$, where $x_A^N \in \mathcal{X}_A^N$ and $x_B^N \in \mathcal{X}_B^N$, the secret key capacity is the supremum of achievable secret key rates. An achievable secret key rate is defined as follows.

Definition 2. *A secret key rate R is achievable if for any $\epsilon > 0$ and N sufficiently large, we have:*

$$NR \log |\mathcal{K}| - H(f(X_A^N)) \leq \epsilon, \tag{17}$$

$$\Pr\left[f(X_A^N) \neq f(g_B(X_B^N, g_A(X_A^N)))\right] < \epsilon, \tag{18}$$

$$\frac{1}{N} I(f(X_A^N); g_A(X_A^N)) \leq \epsilon. \tag{19}$$

The first inequality implies that the secret key is nearly uniformly distributed. The second inequality upper bounds the probability of error in key recovery. The final inequality is the secrecy guarantee, i.e., that the public message tells you little about the key.

The above definitions are often stated for a setting in which an attacker (Eve) has access to a correlated measurement of the source *as well as* the public message. We do not include this possibility in the definitions as stated herein due to the source of randomness we study. We will characterize secret key capacity for an OFDM system where the correlated observations X_A^N and X_B^N are functions of the underlying channel law (the H_n or the h_ℓ of Sec. II). In a rich scattering environment the channel law between two users changes utterly if either moves more than a few wavelengths (a few centimeters for an OFDM system). Therefore an eavesdropper would have to be positioned extremely close to either Alice or Bob to get useful channel observations. This is one of the inherent strengths of this source of randomness – it is difficult to eavesdrop. And for this reason we ignore the possibility of eavesdropping throughout the rest of the paper. (In contrast, the public message is easy to intercept, and so we must assume Eve has knowledge of that message.)

In [6] the following theorem is shown

Theorem 1. *For a discrete memoryless source $p_{X_A^N, X_B^N}(x_A^N, x_B^N)$ the secret key capacity is*

$$C = \lim_{N \to \infty} \frac{1}{N} I(X_A^N; X_B^N), \tag{20}$$

assuming the limit exists.

B. Measurement model

The sources of randomness we work with in the paper are noisy measurements of the channel coefficients. Alice and Bob each sends an identical and known sounding signal $s(t)$ to the other. For simplicity we assume each signal coefficient $s_n = 1$. (Equal-power sounding is known not always to be the best choice, see [8].) We assume that the channel remains static during this two-way training. The period in which a wireless channel is roughly static is termed the *coherence period*. Thus, this two-way training is assumed to occur within a single coherence period.

Under this channel assumption we model Alice and Bob's measurements as

$$\begin{aligned} H_{A,n} &= H_n + w_{A,n} \\ H_{B,n} &= H_n + w_{B,n}, \end{aligned} \tag{21}$$

respectively, where $w_{A,n}$, $w_{B,n} \sim \mathcal{CN}(0, \sigma_W^2)$ are independent sources of noise. We notice that the phase offset caused

by the local oscillators may add extra noise to the measurement [25], [26], [36]. We defer the discussion of phase offset to the end of this section.

The frequency domain correlation coefficient between Alice and Bob's observation at n^{th} tone can be shown to be :

$$\rho_f = \frac{SNR_f}{1+SNR_f}. \tag{22}$$

Note that the correlation ρ_f between $H_{A,n}$ and $H_{B,n}$ is equal to the correlation between $\Re(H_{A,n})$ and $\Re(H_{B,n})$ and is also equal to that between $\Im(H_{A,n})$ and $\Im(H_{B,n})$. We can also consider the time domain observation as:

$$\begin{aligned} h_{A,\ell} &= \Re(h_{A,\ell}) + j\Im(h_{A,\ell}) = h_\ell + n_{A,\ell} \\ h_{B,\ell} &= \Re(h_{B,\ell}) + j\Im(h_{B,\ell}) = h_\ell + n_{B,\ell}, \end{aligned} \tag{23}$$

where $h_\ell \sim \mathcal{CN}(0, \sigma_h^2(\ell))$ is the sampled channel coefficient and $n_{B,\ell}$, $n_{A,\ell} \sim \mathcal{CN}(0, \sigma_W^2)$ are the noises. Similar to the correlation in frequency domain, the correlation coefficient in ℓ^{th} sampled channel coefficient is given as:

$$\rho_\tau(\ell) = \frac{SNR_\tau(\ell)}{1+SNR_\tau(\ell)}. \tag{24}$$

Note again that the correlation coefficient $\rho_\tau(\ell)$ between $h_{A,\ell}$ and $h_{B,\ell}$ is equal to the correlation coefficient between $\Re(h_{A,\ell})$ and $\Re(h_{B,\ell})$ or equivalently equal to that between $\Im(h_{A,\ell})$ and $\Im(h_{B,\ell})$.

To get to the long block-lengths possibly required to approach secret key capacity, we repeat this two-way channel sounding across multiple channel coherence periods. The channel is assumed to be independently and identically distributed across coherence periods. Say that within each period Alice and Bob generate channel observations $h_{A,\ell}$ and $h_{B,\ell}$, respectively, for $\ell = 1, 2, \ldots, L$. Further, say they do this for n coherence periods yielding measurements $h_{A,\ell}[i]$ and $h_{B,\ell}[i]$ for $i = 1, 2, \ldots, n$. They stack their observations into the length-N real vectors, where $N = 2nM$ as follows:

$$X_A^N = \begin{bmatrix} \Re(h_{A,1}[1]) \\ \Im(h_{A,1}[1]) \\ \vdots \\ \Re(h_{A,L}[1]) \\ \Im(h_{A,L}[1]) \\ \Re(h_{A,1}[2]) \\ \vdots \\ \Im(h_{A,L}[n]) \\ 0 \\ \vdots \\ 0 \end{bmatrix}, \quad X_B^N = \begin{bmatrix} \Re(h_{B,1}[1]) \\ \Im(h_{B,1}[1]) \\ \vdots \\ \Re(h_{B,L}[1]) \\ \Im(h_{B,L}[1]) \\ \Re(h_{B,1}[2]) \\ \vdots \\ \Im(h_{B,L}[n]) \\ 0 \\ \vdots \\ 0 \end{bmatrix}, \tag{25}$$

where the padding is with $2nM - 2nL = 2n(M-L)$ zeros. These are the degrees of freedom lost due to the fact that the last $M-L$ coefficients in each block are zero, cf. (9). Were the approximation that the last $M-L$ coefficients in each block were zero to be exact, then due to the i.i.d. assumption across coherence blocks, the limit in (20) would exist and would evaluate to

$$C = \lim_{N\to\infty} \frac{1}{N} I(X_A^N; X_B^N) = \frac{1}{2M} I(h_A^L; h_B^L) \tag{26}$$

where h_A^L and h_B^L are, respectively, the length-L complex vectors of observations made by Alice and Bob. While the definitions provided in Sec. III-A are for finite alphabets, the extension to continuous alphabets follows from standard limiting arguments.

C. Phase Offset

We have thus far implicitly assumed the perfect synchronization between Alice and Bob. In practice, however, Alice and Bob measured channel parameters may be effected by the phase offset caused by the local oscillators of both transmitters. Since phase synchronization is not perfect, there is a phase offset during each channel sounding. Furthermore, the frequency generated by local oscillators continuously fluctuates (or drifts) around its center frequency, causing a time dependent phase drift. There are many existing techniques developed to mitigate the effect of such phase offset (see [36], [26] and the references therein).

Since the signal duration is very small in a channel training, we assume that during each channel sounding phase offset caused by oscillator frequency drift is negligible, i.e., the phase offset is time invariant. However we do not assume it is negligible across channel trainings, i.e., between coherence intervals. Denote the phase offset caused by Alice and Bob's local oscillators as θ_A and θ_B respectively. The offsets can be incorporated into Alice's and Bob's measurements as $h_A^L e^{j\theta_A}$ and $h_B^L e^{j\theta_B}$ cf. (8). Since phase offset is differential, without the loss of generality, we can incorporate the error into Bob's measurement and write h_A^L and $h_B^L e^{j\theta}$ with $\theta = \theta_B - \theta_A$. Then the unnormalized secret key capacity in (26) becomes $I(h_A^L; h_B^L e^{j\theta})$.

We show that by exploiting the channel diversity, one can mitigate the effect on the secret key capacity caused by phase offset. First, note that

$$\begin{aligned} I(h_B^L e^{j\theta}; h_A^L, e^{j\theta}) &= I(h_B^L e^{j\theta}; h_A^L) + I(h_B^L e^{j\theta}; e^{j\theta}|h_A^L) \\ &= I(h_B^L e^{j\theta}; e^{j\theta}) + I(h_B^L e^{j\theta}; h_A^L|e^{j\theta}). \end{aligned}$$

Then we can write:

$$\begin{aligned} I(h_B^L e^{j\theta}; h_A^L) =& I(h_B^L e^{j\theta}; h_A^L|e^{j\theta}) + I(h_B^L e^{j\theta}; e^{j\theta}) \\ & - I(h_B^L e^{j\theta}; e^{j\theta}|h_A^L) \\ =& I(h_B^L; h_A^L) + I(h_B^L e^{j\theta}; e^{j\theta}) - I(h_B^L e^{j\theta}; e^{j\theta}|h_A^L) \\ \overset{(a)}{\geq}& I(h_B^L; h_A^L) - I(h_B^L e^{j\theta}; e^{j\theta}|h_A^L). \\ =& I(h_B^L; h_A^L) - I(e^{j\theta}; h_A^L, h_B^L e^{j\theta}). \end{aligned} \tag{27}$$

Inequality (a) is equality ($I(h_B^L e^{j\theta}; e^{j\theta}) = 0$) if h_B^L is circularly symmetric complex Gaussian vector since h_B^L and $h_B^L e^{j\theta}$ have the same distribution. The last equality follows because $e^{j\theta}$ is independent of h_A^L. The second term on the right hand side of (27), $I(e^{j\theta}; h_A^L, h_B^L e^{j\theta})$, is the secret key capacity loss caused by the phase offset and it is the decrease in uncertainty about the unknown offset $e^{j\theta}$ given the knowledge of h_A^L and $h_B^L e^{j\theta}$ as measured in bits. Note that because h_B^L and $h_B^L e^{j\theta}$ have the same distribution nothing can be learned about θ by observing $h_B^L e^{j\theta}$ only. However in combining with the knowledge of h_A^L one can better estimate θ because

$\angle h_B^L e^{j\theta} = \angle h_B^L + \theta$ and $\angle h_B^L$, $\angle h_A^L$ are dependent random variables. Thus we get L independent looks at θ with additive noise (since h_A^L and h_B^L each has L independent entries). Note that because of the additive noise, it is impossible to estimate θ with infinite precision.

Since θ is a scalar the loss term does not scale linearly in L. By the Cramér-Rao bound we know that variance of the estimate of θ can drop at most as $\frac{1}{L}$ which means for general distribution the loss should scale as $\log L$. In other words, as L becomes larger while one can potentially get better estimate of θ from channel observations, the loss is scaling more slowly than the gain from the first term on the right hand side of (27), which scales linearly in L. This supports our claim that channel diversity should be exploited, both as a way to boost secret key capacity and to mitigate the phase offset.

Later in Sec. V we will show how the LDPC design can be adapted to perform the estimation of phase offset.

IV. Secret key capacity calculations

We are now in position to evaluate the secret key capacity for various channels of interest. In Sec. IV-A we first do this for the general OFDM model of time-domain channel coefficients. Then, to ease analysis, we focus on an idealized model wherein all sampled channel coefficients have the same variance. This simplification allows us to draw a number of general lessons on secret key generation for OFDM channels. In Sec. IV-B we quantify the (quite large) reduction in secret key rate when only received signal strength indicator (RSSI) information is available, as opposed to full CSI. In Sec. IV-C we discuss generating keys separately from the amplitude and phase of the CSI, as opposed to the real and imaginary parts.

A. Secret key capacity based on CSI

We now evaluate (26) in terms of the SNR of the channel. Due to the fact that h_A^L and h_B^L are jointly complex Gaussian and i.i.d. in time, we have

$$C \approx -\frac{1}{2M}\sum_{\ell=0}^{L-1}\log\left[1-\left(\frac{SNR_\tau(\ell)}{1+SNR_\tau(\ell)}\right)^2\right], \tag{28}$$

where the approximation follows from the fact that the last $M-L$ sampled coefficients are approximately zero. If the sampled coefficients have equal variance, the capacity simplifies to

$$C \approx -\frac{L}{2M}\log\left[1-\left(\frac{SNR_\tau}{1+SNR_\tau}\right)^2\right]. \tag{29}$$

Note that the correlation coefficient in time relates to that in frequency as:

$$\rho_\tau \approx \frac{M\cdot SNR_f}{L+M\cdot SNR_f} = \frac{M\rho_f}{L+(M-L)\rho_f}. \tag{30}$$

In the remainder of this section we focus on an idealized model wherein all sampled channel coefficients have the same variance. We let $h_{A,\ell}$, $h_{B,\ell} \sim \mathcal{CN}(0,\sigma^2)$ where $\sigma^2 = \sigma_h^2 + \sigma_W^2$. Note that $\Re(h_{A,\ell})$, $\Re(h_{B,\ell})$ have correlation coefficient ρ_τ defined in (30) and $\Im(h_{A,j})$, $\Im(h_{A,j})$ also have the same correlation coefficient ρ_τ. The secret key capacity between Alice and Bob now reduces to (29).

B. Secret key generation based on measurements of RSSI

In this section we compare the secret key capacity given sampled channel coefficients (29) to the secret key capacity if only receiver signal strength indicator (RSSI) values are available. Since RSSI summarizes the true vector of channel state information, there will clearly be a reduction in secret key capacity if only RSSI values are made available. In fact the reduction is dramatic. From a technological point of view, most off-the-shelf wireless transceivers make only RSSI values available to the upper layers, not the channel state information. This section demonstrates that making full CSI available would greatly help the ability to generate secret keys.

To calculate the secret key capacity based on RSSI values, let R_A and R_B denote the RSSI values received by Alice and Bob. In an OFDM system, the RSSI takes the form [37]:

$$R_A = \sum_{\ell=0}^{L-1}|h_{A,\ell}|^2 = \sum_{\ell=0}^{L-1}\left[|\Re(h_{A,\ell})|^2+|\Im(h_{A,\ell})|^2\right] = \sum_{\ell=0}^{2L-1}X_{A,\ell}^2,$$

where

$$X_{A,\ell} = \begin{cases} |\Re(h_{A,\ell})|^2 & \text{if} \quad 0\le\ell\le L-1 \\ |\Im(h_{A,\ell-L})|^2 & \text{if} \quad L\le\ell\le 2L-1 \end{cases}$$

The quantities R_B and $X_{B,\ell}$ are defined similarly. Further, $X_{A,\ell}$ and $X_{B,\ell}$ are $\mathcal{N}(0,\frac{\sigma^2}{2})$ Gaussian random variables with $\rho_\tau = E[X_{A,\ell}X_{B,\ell}]$ for all ℓ.

Both R_A and R_B are non-standard chi-square distributed random variables with $2L$ degree of freedom. The joint probability density function of a pair of chi-square random variables is given in Theorem 2.1 in [38] and we use it to numerically calculate the mutual information between R_A and R_B, denoting the secret key capacity calculated as:

$$C_R = \frac{1}{2M}I(R_A;R_B). \tag{31}$$

When L is large, R_A and R_B can be well approximated as Gaussian random variables $\mathcal{N}(2L,4L)$ due to the central limit theorem. The mean and variance for R_A and R_B can be calculated as $E[R_A] = \sum_{\ell=0}^{2L-1}E[X_{A,\ell}^2]$ and $var(R_A) = \sum_{\ell=0}^{2L-1}var(X_{A,\ell}^2)$ using the identities $E[X_{A,\ell}^2] = 1$, $E[X_{A,\ell}^4] = 3$, and $E[(X_{A,\ell}^2 - E[X_{A,\ell}^2])^2] = 2$, which follow from the variance normization. The correlation coefficient between R_A and R_B is

$$\begin{aligned}\rho_R &= \frac{E[(R_A-2L)(R_B-2L)]}{4L} \\ &= \frac{E[(X_{A,\ell}^2-1)(X_{B,\ell}^2-1)]}{2},\end{aligned} \tag{32}$$

where the joint moment generating function of $X_{A,\ell}$ and $X_{B,\ell}$ is:

$$M(s_1,s_2) = E[e^{s_1X_{A,\ell}+s_2X_{B,\ell}}] = e^{[\frac{1}{2}(s_1^2+2\rho_\tau s_1s_2+s_2^2)]}. \tag{33}$$

We calculate the joint moment $E[X_{A,\ell}^2X_{B,\ell}^2]$ by taking second order partial derivatives of $M(s_1,s_2)$ respect to s_1 and s_2 and evaluate the result at $s_1=0$, $s_2=0$. Equation (32) can be reduced to:

$$\rho_R = \rho_\tau^2, \tag{34}$$

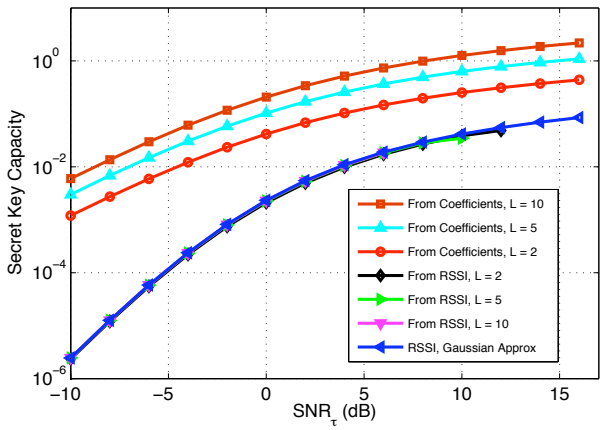


Fig. 1. Secret key capacity when L = 2, 5, and 10. M = 10

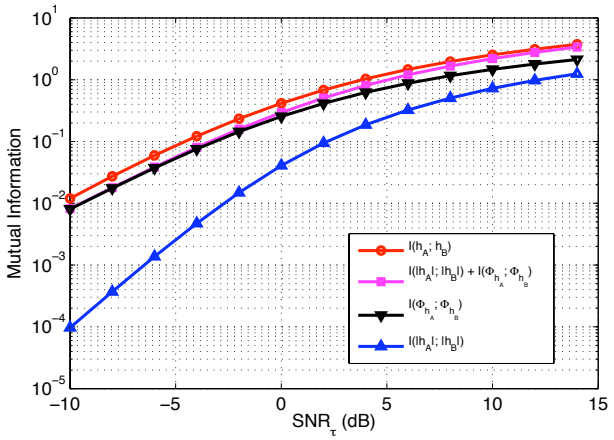


Fig. 2. Comparison of the secret key capacity to the sum of the mutual information between the magnitude of the observations and that between the phases.

and the secret key capacity based on RSSI under Gaussian approximation is then:

$$C_R = \frac{1}{4M} \log \left(\frac{1}{1-\rho_\tau^4} \right). \tag{35}$$

Observe from (35) that the secret key capacity does not depend on L. In other words, at a given SNR_τ, while the capacity between coefficients increases linearly with L as shown in equation (29), the capacity between RSSI stays the same. This is because there is only one single RSSI value regardless the number of observations. In Fig. 1, we compare the capacity obtained from channel coefficients and from RSSI for $L = 2, 5$ and 10 with $M = 10$. The secret key capacity between the channel coefficients is calculated using (29) and that between RSSI is calculated both using numerical (31) and Gaussian approximation (35). We first note that the secret key capacity obtained from the channel coefficients increases with L, whereas that based on RSSI stays constant. We also note that the Gaussian approximation is quite accurate, even when L is rather small.

C. Representing complex channel coefficients by their real-and-imaginary parts or by their magnitude-and-phase

Recall that the secret key capacity (26) is the mutual information between the sampled channel coefficients observed by Alice and Bob. In this section we show this capacity is at least as large as the sum of the mutual informations between the magnitudes of the channel coefficients and that between the phases of the channel coefficients. This is because while marginally the channel coefficients observed by Alice and Bob are circularly symmetric (and thus their magnitude and phase are independent), the correlation between Alice and Bob's channel coefficients means there is dependence between Alice's phase and Bob's magnitude and vice-versa. Thus, the secret key should not be generated by treating phase and magnitude separately. On the other hand, the real parts of Alice and Bob's coefficients are independent of the imaginary parts. Thus, without loss of capacity the key can be generated treating the real and imaginary parts of each pair of observations as separate pieces of independent randomness. This is the reason behind our choice of definition of X_A^N and X_B^N in (25).

This idea is encapsulated in the following theorem. For simplicity (and because the sampled channel coefficients are independent) we focus on a single pair of observations, h_A and h_B.

Theorem 2. *If h_A, and $h_B \sim \mathcal{CN}(0, \sigma^2)$ are jointly complex Gaussian random variables, we have:*

$$\begin{aligned} I(h_A; h_B) &= I(\Re(h_A); \Re(h_B)) + I(\Im(h_A); \Im(h_B)) \\ &\geq I(|h_A|; |h_B|) + I(\Phi_{h_A}; \Phi_{h_B}). \end{aligned}$$

Proof: See Appendix A. ∎

In Figure 2 we illustrate this result for a range of SNR. We plot the capacity $I(h_A; h_B)$, $I(|h_A|; |h_B|) + I(\Phi_{h_A}; \Phi_{h_B})$, as well as the two terms of the latter, $I(\Phi_{h_A}; \Phi_{h_B})$ and $I(|h_A|; |h_B|)$. The gap to capacity is evident at all SNR. It is also worthwhile to note that most of the information is in the phase information, $I(|h_A|; |h_B|)$ is much smaller. This is another illustration of the lesson of Sec. IV-B as the magnitude information is the RSSI of this example. We reiterate that the reason for the gap to capacity is that the pairs $(|h_A|, |h_B|)$ is not statistically independent of (Φ_{h_A}, Φ_{h_B}) due to the correlation between real and imaginary parts of h_A and h_B.

V. Design and Algorithms

In this section we describe a key reconciliation system based on low-density parity-check (LDPC) codes. The basic idea behind our design is the following. Alice and Bob have correlated observation X_A^N and X_B^N, cf. (25), and shared knowledge of a LDPC code. First, Alice makes a quantized version $X_{A,Q}^N$ of her observation X_A^N. Generally $X_{A,Q}^N$ will *not* be a codeword of the LDPC code, but it will always be an element of some coset of the code. She determines this coset by calculating the *syndrome* of her observation, which she sends to Bob. Thus, the syndrome is the public message in (15). By itself the syndrome reveals little information about the source since there are so many sequences in the coset. This

is why this construction satisfies the secrecy condition of (19). However, with knowledge of the coset and of his observation X_B^N, Bob can "de-noise" X_B^N to recover $X_{A,Q}^N$ by decoding the LDPC code with respect to the known coset in which $X_{A,Q}^N$ lies while treating X_B^N as a noisy observation of $X_{A,Q}^N$. All cosets inherit the distance properties of the LDPC code, which gives the needed robustness to the random differences between X_A^N and X_B^N. It should be noted that this is a well-understood method for tackling these problems, see, e.g., [39]. Our contribution is really the prototyping of this system for the random source of interest (wireless channels) and some design for non-binary quantization.

In Sec. V-A we provide some background on LDPC codes and how they fit into the key generation framework of Def. 1. In Sec. V-B we describe the algorithm implemented for non-binary (four-level) quantization.

A. Background, setup, and secrecy analysis

A length-N rate-R LDPC code over $GF(q)$ is characterized by its $m \times N$ parity check matrix $\mathbf{P}$ with elements drawn from $GF(q)$ where $R = (1 - m/N)\log_2(q)$ bits per channel use. The parity check matrix of a LDPC code is low-density in the sense that the number of non-zero elements of each row is upper bounded by some constant, regardless of the block-length N. Thus, most elements of $\mathbf{P}$ are zero. A *regular* LDPC code has a constant row-weight (number of non-zero elements) and a constant column-weight. An *irregular* LDPC code has a set of row and column weights, where the fraction of each is specified by a degree distribution polynomial.

In producing $X_{A,Q}^N$ Alice has a choice of quantization. In our design she performs scalar quantization, quantizing each element of X_A^N independently. Further, we study two quantization alphabets: the first where each of the N elements of $X_{A,Q}^N$ is binary, the second where each is quaternary. Bob may choose also to quantize his observations prior to decoding, but there will be a loss in information (and thus performance) if he does so. If Bob also quantizes his observations, he is said to perform "hard" decoding, while if he does not he is said to perform "soft" decoding.

Alice creates her public message by multiplying her observation $X_{A,Q}^N$ with $\mathbf{P}$ to produce the length-m syndrome S^m, $S^m = \mathbf{P}X_{A,Q}^N$, where $m = N[1 - R/\log_2(q)]$. Within each coset there are $2^{N\log_2(q)(1-m/N)} = 2^{NR}$ sequences. As long as $NR < I(X_{A;Q}^N; X_B^N)$ then recovery of $X_{A,Q}^N$ (decoding) will be reliable. It can be shown that, $H(X_{A,Q}^N|S^m)$, the uncertainty in $X_{A,Q}^N$ given the knowledge of the public message S^m is at least NR. This means that the uncertainty in $X_{A,Q}^N$ given knowledge of the public message S^m is exactly the same as the size of the coset. Thus, if the key extraction function $f(\cdot)$ first quantizes X_A^N to get $X_{A,Q}^N$ and then sets the key to be equal to the index that identifies $X_{A,Q}^N$ within the coset of the LDPC code in which it lies, the mutual information of this index with S^m will be arbitrarily small, satisfying the secrecy condition (19). Finally, since $R < (1/N)I(X_{A,Q}^N; X_B^N)$ for successful recovery, we get the upper bound on the achievable secrecy rate approaches (20) as the quantization gets increasingly fine.

B. Design based on non-binary LDPC codes

In Sec. VI-B we present simulation results for two key generation systems based upon LDPC codes. In the first Alice uses binary quantization to produce $X_{A,Q}^N$ and in the second she uses four-level quantization. In this section we describe the design only for the four-level (non-binary) quantization as the one for binary quantization is based upon standard LDPC decoding techniques.

To simplify notation, in this section we use x_i to represent the ith element of Alice's quantized observation $X_{A,Q}^N$ and y_i to represent the ith element of Bob's (not necessarily quantized) observation X_B^N. As our discussion is for four-level design, $x_i \in \{0, 1, 2, 3\}$. Similarly s_i is the ith element of S^m, also in $\{0, 1, 2, 3\}$ as are all elements of $\mathbf{P}$. To simplify the design, rather than working with a code with elements in $GF(4)$ we split each x^N into bit planes, representing each x_i by a pair of binary symbols $x_{i,M}$ and $x_{i,L}$, each taking the respective value in $\{0, 1\}$ that satisfies

$$x_i = x_{i,L} + 2x_{i,M}. \tag{36}$$

We can now apply a pair of length-N binary LDPC code, one to each bit plane, or a length-$2N$ binary LDPC code to the concatenation of the bit planes. We implemented both and, while the latter generally has the higher performance (though not by too much), the former allows more flexibility (e.g., in reconstructing only the most significant bit plane or sequential reconstruction) and is slightly simpler to implement. We choose to present our results on the former, using $\mathcal{C}_\alpha$, $\mathbf{P}_\alpha$, and $s_\alpha^{m_\alpha}$ to represent, respectively, the code, the parity check matrix, and the syndrome associated with x_α^N – the sequence of concatenated $x_{i,\alpha}$ where $\alpha \in \{L, M\}$. We note that $\mathcal{C}_M$ and $\mathcal{C}_L$ need not be the same rate so $m_M \neq m_L$ in general. However, in all our simulations we choose $\mathbf{P}_M = \mathbf{P}_L$, where equality is element-wise, so $\mathcal{C}_M = \mathcal{C}_L$. Recall that the syndrome is calculated as $s_\alpha^{m_\alpha} = \mathbf{P}_\alpha x_\alpha^N$.

To visualize the two binary LDPC codes and to see how to relate them to the observation y_i we depict the constraints involved in the key generation process in Fig. 3 using a factor graph [40]. The factor nodes F_i constrain the triplet of variables $(x_i, x_{i,L}, x_{i,M})$ to satisfy the relationship of (36). In particular,

$$F_i(x_i, x_{i,M}, x_{i,L}) = \begin{cases} 1, & \text{if} \quad x_i = x_{i,L} + 2x_{i,M} \\ 0, & \text{else} \end{cases}$$

We attempt to recover $X_{A,Q}^N$, based on knowledge of y^N and $S_M^{m_M}$ and $S_L^{m_L}$, by using the sum-product algorithm. In this algorithm messages that approximate conditional probability distributions are iteratively passed along the edges of the factor graph. We use the parallel message passing schedule, have all factor nodes send messages to all variable nodes, and then vice-versa; continuing until either the messages converge or some maximum number of iterations is reached. For more details of these standard aspects of the implementation see [40]. In the remainder of this section we indicate the form of the message updates required for the non-binary case.

We use the following symbols to represent the messages passed. The message sent from node x_i to node F_i and

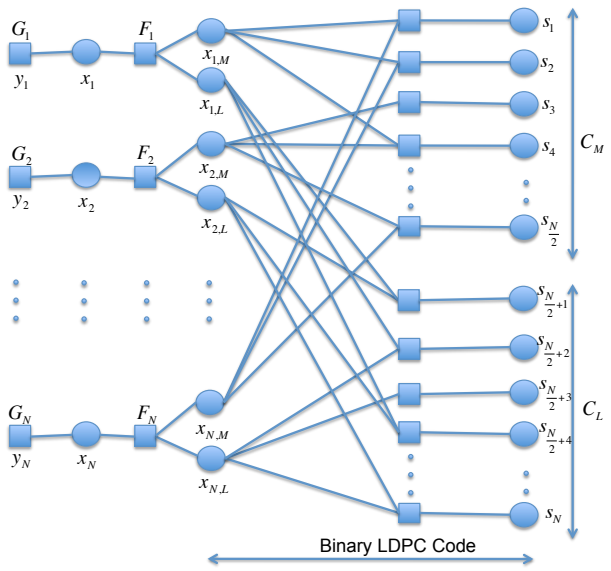


Fig. 3. Factor graph of 4-ary LDPC codes. Nodes $x_{i,M}$ and $x_{i,L}$ connect to the check nodes of different binary LDPC code. They are connected by local function F_i which regulates them according to the value of x_i.

from node F_i to x_i are, respectively, denoted $\mu_{x_i\to F_i}(x_i)$ and $\mu_{F_i\to x_i}(x_i)$. We use $\mathcal{N}(p)$ to denote the neighbors of a given node p. The summary operator $\sum_{\sim\{p\}}$ means summation over all variables *except* p and the notation $\mathcal{N}(p)\backslash\{q\}$ means the set of neighbors of p *except* q. We now detail the form the general sum-product update rules specialized for our problem.

The message passed from variable node x_i to F_i are calculated as

$$\begin{aligned}\mu_{x_i\to F_i}(x_i) &= \prod_{t\in\mathcal{N}(x_i)\backslash\{F_i\}} \mu_{t\to x_i}(x_i)\\ &= \mu_{y_i\to x_i}(x_i).\end{aligned}$$

As there is no marginalization at variable node x_i, the message passed to F_i is the same as the incoming message from y_i,

$$\mu_{y_i\to x_i}(x_i) = G_i(x_i),$$

where the local function $G_i(x_i)$ is the channel evidence

$$G_i(x_i) = p_{X_i|Y_i}(x_i|y_i).$$

The messages passed from factor node F_i to each of the two binary variable nodes $x_{i,\alpha}$ where $\alpha\in\{M,L\}$ is calculated as

$$\begin{aligned}&\mu_{F_i\to x_{i,\alpha}}(x_{i,\alpha})\\ &= \frac{1}{Z}\sum_{\sim\{x_{i,\alpha}\}}\left(F_i(x_i,x_{i,M},x_{i,L})\prod_{t\in\mathcal{N}(F_i)\backslash\{x_{i,\alpha}\}}\mu_{t\to F_i}(t)\right),\end{aligned}$$

where Z is a normalization factor,

$$Z = \sum_{x_{i,\alpha}}\sum_{\sim\{x_{i,\alpha}\}}\left(F_i(x_i,x_{i,M},x_{i,L})\prod_{t\in\mathcal{N}(F_i)\backslash\{x_{i,\alpha}\}}\mu_{t\to F_i}(t)\right).$$

For example:

$$\begin{aligned}&\mu_{F_i\to x_{i,M}}(1)\\ &= \frac{1}{Z}\Big(\mu_{x_i\to F_i}(2)\mu_{x_{i,L}\to F_i}(0)+\mu_{x_i\to F_i}(3)\mu_{x_{i,L}\to F_i}(1)\Big),\\ &\mu_{F_i\to x_{i,M}}(0)\\ &= \frac{1}{Z}\Big(\mu_{x_i\to F_i}(1)\mu_{x_{i,L}\to F_i}(1)+\mu_{x_i\to F_i}(0)\mu_{x_{i,L}\to F_i}(0)\Big),\end{aligned}$$

where Z is given by

$$\begin{aligned}Z = &\mu_{x_i\to F_i}(2)\mu_{x_{i,L}\to F_i}(0)+\mu_{x_i\to F_i}(3)\mu_{x_{i,L}\to F_i}(1)\\ &+\mu_{x_i\to F_i}(1)\mu_{x_{i,L}\to F_i}(1)+\mu_{x_i\to F_i}(0)\mu_{x_{i,L}\to F_i}(0).\end{aligned}$$

The log-likelihood for $x_{i,M}$ is $\log\left(\frac{\mu_{F_i\to x_{i,M}}(0)}{\mu_{F_i\to x_{i,M}}(1)}\right)$ which serves as the channel evidence for the binary code $\mathcal{C}_M$. Similarly, variable node $x_{i,L}$ calculates the channel evidence for $\mathcal{C}_L$. Based on these messages, the messages passed in the LDPC codes are standard messages where the $s_\alpha^{m_\alpha}$ make sure that the decoding is performed with respect to the correct cosets. This aspect is the same as when LDPC codes are used in Slepian-Wolf distributed source coding problems, e.g., see [41]. The messages passed from the LDPC codes back to the F_i are $\mu_{x_{i,M}\to F_i}(x_{i,M})$ and $\mu_{x_{i,L}\to F_i}(x_{i,L})$.

Finally, the message passed from F_i to variable node x_i is calculated as

$$\begin{aligned}&\mu_{F_i\to x_i}(x_i)\\ &= \frac{1}{Z}\sum_{\sim\{x_i\}}\left(F_i(x_i,x_{i,M},x_{i,L})\prod_{t\in\mathcal{N}(F_i)\backslash\{x_i\}}\mu_{t\to F_i}(t)\right)\\ &= \frac{1}{Z}\sum_{\sim\{x_i\}}\Big(F_i(x_i,x_{i,M},x_{i,L})\mu_{x_{i,M}\to F_i}(x_{i,M})\mu_{x_{i,L}\to F_i}(x_{i,L})\Big),\end{aligned}$$

where Z is the corresponding normalization factor. For example:

$$\mu_{F_i\to x_i}(2) = \frac{1}{Z}\Big(\mu_{x_{i,M}\to F_i}(1)\mu_{x_{i,L}\to F_i}(0)\Big),$$

where Z is

$$\begin{aligned}Z = &\mu_{x_{i,M}\to F_i}(0)\mu_{x_{i,L}\to F_i}(0)+\mu_{x_{i,M}\to F_i}(1)\mu_{x_{i,L}\to F_i}(0)\\ &+\mu_{x_{i,M}\to F_i}(0)\mu_{x_{i,L}\to F_i}(1)+\mu_{x_{i,M}\to F_i}(1)\mu_{x_{i,L}\to F_i}(1).\end{aligned}$$

Eventually, the messages either converge or the maximum iteration count is reached. In our simulations we set this maximum to 50 iterations. When the messages converge the marginals are computed as the following up to a scaling factor.

$$\Pr[x_i=a]\propto\mu_{y_i\to x_i}(a)\mu_{F_i\to x_i}(a),$$

where $a\in\{0,1,2,3\}$. The algorithm sets its estimates symbol-by-symbol as $\hat{x}_i=\arg\max_a\Pr[x_i=a]$.

We now present the initialization of our algorithm. $GF(4)$ variable nodes x_i are initialized as:

$$\mu_{y_i\to x_i}(x_i) = G_i(x_i),$$

whereas $GF(2)$ variable nodes $x_{i,M}$ are initialized as:

$$\mu_{F_i\to x_{i,M}}(x_{i,M}) = \frac{1}{Z}\sum_{\sim\{x_{i,M}\}}\left(F_i(x_i,x_{i,M},x_{i,L})\prod_{t\in\mathcal{N}(F_i)\setminus\{x_{i,M}\}}\mu_{t\to F_i}(t)\right).$$

At this step the values $x_{i,L}$ can all be set to have equal probability as this is the best estimate $x_{i,L}$ can be set to initially. In other words, the foregoing equation reduces to:

$$\mu_{F_i\to x_{i,M}}(x_{i,M}) = \frac{1}{Z}\sum_{\sim\{x_{i,M}\}}\left(F_i(x_i,x_{i,M},x_{i,L})\mu_{x_i\to F_i}(x_i)\frac{1}{2}\right).$$

Therefore, the message initializing $x_{i,M}$ is $\mu_{F_i\to x_{i,M}}(1) = \frac{1}{Z}\left(\frac{1}{2}\mu_{x_i\to F_i}(2) + \frac{1}{2}\mu_{x_i\to F_i}(3)\right)$. Its corresponding log-likelihood is $\log\left(\frac{\mu_{F_i\to x_{i,M}}(0)}{\mu_{F_i\to x_{i,M}}(1)}\right)$ which serves as the initial channel evidence in $GF(2)$ for $\mathcal{C}_M$. The message initializing $x_{i,L}$ can be similarly derived which serves as the initial channel evidence in $GF(2)$ for $\mathcal{C}_L$.

C. Phase Offset Estimation

As discussed in Sec. III-C, the phase offset during two-way channel training will degrade the quality of the channel measurement. Therefore, one needs to implement phase offset suppression techniques such as phase estimation [26], [36], [42]. In this section, we present a novel approach that incorporates the estimation of phase offset into the design of reconciliation process.

For the ease of presentation, we assume the phase offset is constant across multiple channel trainings. Our idea can easily be extended to the situation where phase offset is time varying. We propose a joint phase offset estimation and reconciliation process, formulated as:

$$(\hat{x}^N,\ \hat{\theta}') = \underset{\{x^N,\theta'\ |\ \mathbf{P}x^N=s^m,\theta'\in[0,2\pi]\}}{\arg\max} p_{X^N|Y^N}(x^N e^{j\theta'}|y^N e^{j\theta}). \tag{37}$$

Incorporating the task of phase offset estimation as in (37) into the reconciliation process puts an extra burden on the codes. To support phase offset estimation, the code rate should be lower. This reduces the cardinality of the coset that specified by the syndrome as is illustrated in Fig. 4. The lower code rate means a lower secrecy rate, reduced by the loss in (27). Fig. 4 depicts the coupling between this lowered rate and the joint decoding problem in (37). If the code rate is lower (a larger syndrome is used as the public message), then for a given optimal θ' parameter in (37) there will be fewer coset elements x^N such that $\mathbf{P}x^N = s^m$ that yields a high probability (right oval in Fig. 4). If the original code rate is used, then there will be many high probability coset elements (left oval in Fig. 4) and the decoding will be erroneous with high probability.

While the above discussion indicates a generic approach, we now show how to integrate this search into our message passing algorithm. We propose a joint phase offset estimation and reconciliation procedure by concatenating an extra variable node θ to all the check nodes $G_i, i = 1, 2, \ldots, N$, where θ denotes the random phase offset between Alice and Bob. We assume the θ is discretized such that it can only take some finite values. Then by passing message to and from variable node θ, one could obtain the estimate of θ. The algorithm works as follows.

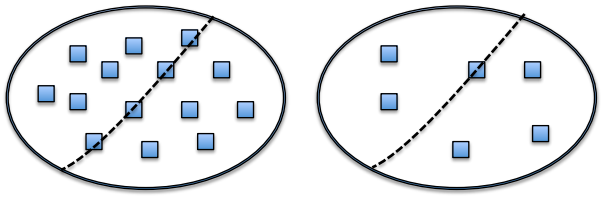


Fig. 4. Cosets of different LDPC code rates are shown as ovals. The one on the left corresponds to higher code rate. It contains many candidate codewords thus (37) may have non-unique solutions. The oval on the right is sparser, corresponding to a lower code rate. Thus it is possible to have a unique solution to (37). Phase rotation θ' in (37) is represented as the dashed line.

The message passed from θ to G_i is

$$\mu_{\theta\to G_i}(\theta) = \prod_{t\in\mathcal{N}(\theta)\setminus G_i}\mu_{t\to\theta}(\theta). \tag{38}$$

The message passed from G_i to x_i is

$$\mu_{G_i\to x_i}(x_i) = \frac{1}{Z}\sum_{\theta}\left(p_{X_i\theta|Y_i}(x_i,\theta|y_i)\mu_{\theta\to G_i}(\theta)\right), \tag{39}$$

where Z is some normalization factor. The message passed from x_i to G_i is

$$\mu_{x_i\to G_i}(x_i) = \mu_{F_i\to x_i}(x_i). \tag{40}$$

Finally, the message passed back to θ is

$$\mu_{G_i\to\theta}(\theta) = \frac{1}{Z}\sum_{x_i}\left(p_{X_i,\theta|Y_i}(x_i,\theta|y_i)\mu_{x_i\to G_i}(x_i)\right), \tag{41}$$

where Z is some constant. To initialize the algorithm, one can choose the uniform distribution over all the values the θ variable can take.

Our design extends to the cases where phase offset varies across multiple channel trainings. One can concatenate multiple θ variables, each connecting to all the check nodes G_i that belong to the same channel training. The actual implementation of this algorithm is left as a future work.

VI. Simulation Results

In this section we provide simulation results and discussion for our proposed secret key generation system.

A. OFDM simulation results

We first show the simulation result of an IEEE 802.11a channel. We simulate the frequency and sampled channel coefficients and their correlation matrices. Then we numerically compute the empirical secret key capacity between Alice and Bob based on our simulated time domain channel coefficients under different channel environment.

In Table. I we list some channel parameters for a typical rich multipath OFDM 802.11a environment [43]. Secret key capacity simulated at a particular SNR_f is also listed for

TABLE I
CHANNEL PARAMETERS AND SECRET KEY CAPACITY

No. of Tones (M)	52
Total Bandwidth	20 MHz
Total Data Bandwidth (W)	16.25 MHz
Signal Duration (T)	3.2 μs
Carrier Frequency Spacing (Δf)	312.5 kHz
Center Carrier Frequency (F)	5.18 GHz
Coherence Time	100 ms
Max Delay Spread ($\tau_{\max}$)	800 ns
Typical Indoor Delay Spread	40 ns - 1 μs
Typical Outdoor Delay Spread	1 μs - 200 μs
Secret Key Capacity (C) at 20 dB	1040 bits/sec

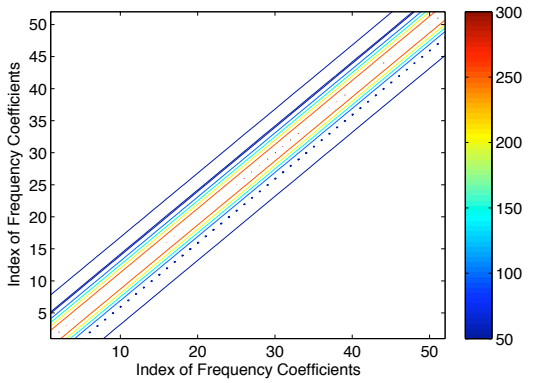
a quick reference. When coherence time is small, the secret key capacity becomes large as new randomness is supplied at higher rate. However, the relationship between secret key capacity and the degree of freedom $L \approx \lceil \tau_{\max} W \rceil$ is more complicated and depends on the operating SNR_f. While the scaling is roughly linear in delay spread and bandwidth there are second order effects that makes the relationship more complicated. This is illustrated in Sec. VI-A2.

1) Channel coefficients simulation: We consider $N_p = 300$ transmission paths and assume the 52 tones all have the same SNR_f, cf. (10). For simplicity, we choose the maximum delay spread $\tau_{\max}$ to be 800 ns so that the degree of freedom (DoF) $L \approx \lceil \tau_{\max} W \rceil = 13$. We reduce the redundancy in the $M = 52$ frequency domain channel coefficients by transforming them into 13 independent sampled channel coefficients. Over each coherence time, we let τ_k be drawn uniformly from 0 to $\tau_{\max}$ and β_k are independent Gaussian random variables whose variances are related to the drawn τ_k through the exponential power-delay profile. We generate 10^6 independent realizations of such channel and construct the contour plots of empirical correlation matrices of frequency domain channel coefficients and sampled channel coefficients as shown in Fig. 5.

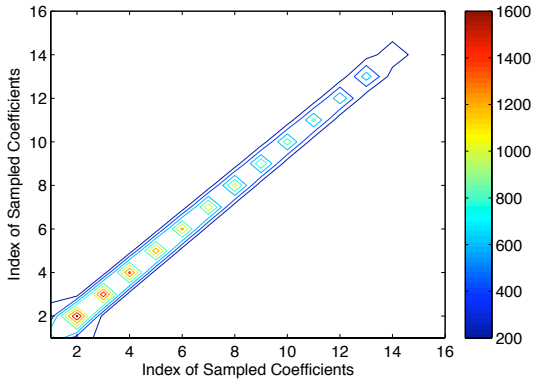
2) Secret key capacity simulation: Secret key capacity can be computed from the first L nonzero sampled channel coefficients using (28). We plot in Fig. 6 the secret key capacity calculated from sampled channel coefficients. Note that the secret key capacity calculated using sampled channel coefficients is an approximation. As we see from Fig. 6, the total number of bits we can obtain per coherence time is as large as $1 \times 52 \times 2 = 104$ bits at 20 dB. It is 1040 bits per second when coherence time is 100 ms.

Simulation in Fig. 6 suggest that there is no single optimal OFDM channel which has the best secret key capacity under any SNR_f: under low SNR_f, one would like the channel to possess fewer degree of freedom; under high SNR_f, one would like the channel to have more degree of freedom. This is analogous to [14] where the authors observe that there is a trade-off between the power per degree of freedom and the number of degree of freedom. The intuition is also related to [44] where it is shown that peaky signal is capacity achieving input to an AWGN fading channel.

One can also compute secret key capacity from frequency domain channel coefficients. Due to page limit constraint we omit the results.



(a) Correlation matrix of frequency channel coefficients



(b) Correlation matrix of sampled channel coefficients

Fig. 5. OFDM channel coefficients simulation. Note that 13 sampled channel coefficients are decorrelated from 52 frequency domain channel coefficients. Note that sampled channel coefficients do not have the same variance.

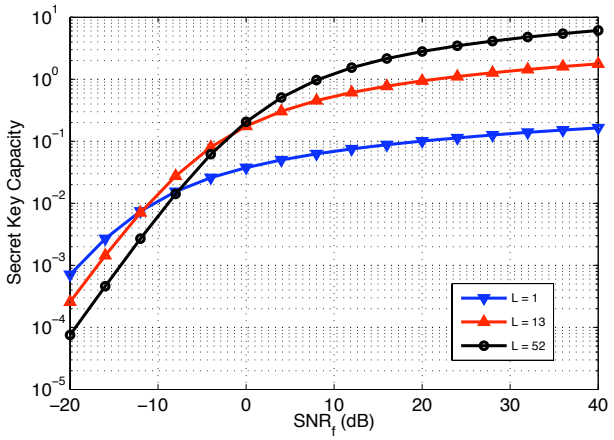


Fig. 6. Secret key capacity of sampled channel coefficients

B. LDPC Performance

In this subsection we simulate the performance of our error correcting code. We allow Alice and Bob to perform multiple channel trainings. There are two ways we simulate the error correction process to reconcile Alice and Bob's measured

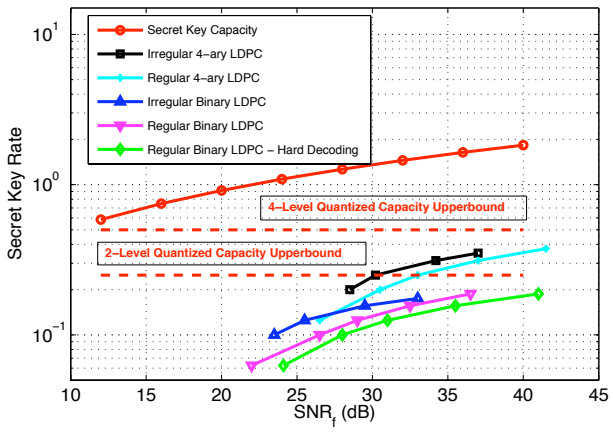


Fig. 7. LDPC performance

channel coefficients. If Bob quantizes his channel coefficients, we term the reconciliation a *hard decoding* process. On the other hand, if Bob keeps his unquantized coefficients such that $\mathcal{Y} = \mathbb{R}$, we term it a *soft decoding* process. In soft decoding, the decoder has access to Bob's full unquantized channel coefficients which improves decoding performance.

We let Alice and Bob perform $n = 30$ independent channel trainings yielding a block length of $N = 30 \times 52 \times 2 = 3120$. One benefit of using a large block length is that LDPC code performs better under longer block lengths. We generate 400 independent realizations of such 30 trainings and aggregate the secret key bit error from the channel trainings of each. For each LDPC code rate, we plot its corresponding SNR which yields approximately 10^{-3} secret key bit error rate. The number of realization is sufficient as 400×3120 is on the order of 10^6 which suffices to assess system performance at bit error rates of 10^{-3}.

We simulate the performance of our error correcting code using the sampled channel coefficients we simulated in Section VI-A1 with $L = 13$. We connect our LDPC simulation with the secret key capacity in Section VI-A2 by putting them in the same plot. We plot the capacity when $L = 13$ and the performance of the binary and non-binary (4-ary) LDPC code in Fig. 7. The irregular LDPC codes are constructed using density evolution technique [45]. We first note that our decoding performance is improved by using soft decoding and it is further improved by using irregular LDPC codes. Non-binary LDPC further improves the performance and approaches the capacity at high SNR_f region. LDPC codes with rate below 0.25 are not simulated as low code rate means less secrecy.

VII. Conclusion and Future Work

We study channel randomness and propose a practical system that generates secret keys from observing the channel randomness. We investigate the secret key capacity shared by two end users and find that secret key generation based on CSI is superior to the key generation based on RSSI. This is because the CSI-based method has the larger secret key capacity. We suggest that modern receiver circuitry should make CSI accessible to upper layer applications. We prove that it is always preferable to use the real and imaginary parts of the sampled channel coefficients, as opposed to using magnitude and phase separately. Our simulation show that it is feasible to base key generation on sampled channel coefficients. Finally, we implement the key generation system based both on regular and irregular LDPC codes.

VIII. Acknowledgement

We would like to thank Vincent Y. F. Tan, Tzu-Han Chou, Jing Yang and Xishuo Liu for their continuous discussion and support. We would also like to thank anonymous reviewers for their feedback and suggestion.

Appendix

A. Proof of Theorem 2

We first show the following lemma.

Lemma 1. *Let X, Y and Z be random variables. If Z is independent either of X or of Y or both, then*

$$I(X;Y|Z) \geq I(X;Y),$$

where equality holds if and only if Z is independent of (X,Y).

Proof: Suppose Z is independent of X. Follow the definition of mutual information, we have the following,

$$\begin{aligned} I(X;Y|Z) &= \mathcal{H}(X) - \mathcal{H}(X|Y,Z) \\ &\geq \mathcal{H}(X) - \mathcal{H}(X|Y) \\ &= I(X;Y), \end{aligned}$$

where $\mathcal{H}(\cdot)$ denotes the differential entropy. Equality holds if Z is independent of (X,Y). ∎

We now prove the theorem.

Proof: We first prove the inequality in the theorem

$$\begin{aligned} &I(h_A;h_B) \\ &= I(|h_A|, e^{j\phi_A}; h_B) \\ &\overset{(a)}{=} I(|h_A|;h_B) + I(e^{j\phi_A};h_B\,|\,|h_A|) \\ &\overset{(b)}{\geq} I(|h_A|;h_B) + I(e^{j\phi_A};h_B) \\ &= I(|h_A|;|h_B|,e^{j\phi_B}) + I(e^{j\phi_A};|h_B|,e^{j\phi_B}) \\ &\overset{(c)}{=} I(|h_A|;|h_B|) + I(|h_A|;e^{j\phi_B}\,|\,|h_B|) \\ &\quad + I(e^{j\phi_A};|h_B|) + I(e^{j\phi_A};e^{j\phi_B}\,|\,|h_B|) \\ &\overset{(d)}{\geq} I(|h_A|;|h_B|) + I(|h_A|;e^{j\phi_B}) \\ &\quad + I(e^{j\phi_A};|h_B|) + I(e^{j\phi_A};e^{j\phi_B}) \\ &= I(|h_A|;|h_B|) + I(|h_A|;\phi_B) + I(\phi_A;|h_B|) + I(\phi_A;\phi_B) \\ &\overset{(e)}{\geq} I(|h_A|;|h_B|) + I(\phi_A;\phi_B), \end{aligned}$$

where (a) and (c) follow from the chain rule of mutual information, (b) follows because $|h_A|$ is independent of ϕ_A (cf. Lemma 1), (d) follows because $|h_B|$ is independent of ϕ_B and (e) follows because mutual information is non-negative. This proves the inequality in the theorem.

The first equality in the theorem is proved by showing that the density function of (h_A, h_B) can be factored into

the product of density functions of $(\Re(h_A), \Re(h_B))$ and $(\Im(h_A), \Im(h_B))$. ■

REFERENCES

[1] Y. Liang, H. V. Poor, and S. Shamai, *Information Theoretic Security*, vol. 5. Foundations and Trends in Communications and Information Theory, 2009.

[2] A. D. Wyner, "The wire-tap channel," tech. rep., Oct. 1975.

[3] I. Csiszár and J. Körner, "Broadcast channels with confidential messages," *IEEE Trans. Inform. Theory*, vol. IT-24, pp. 339–348, May 1978.

[4] M. Bloch, J. Barros, M. R. D. Rodrigues, and S. W. McLaughlin, "Wireless information-theoretic security," *IEEE Trans. Inform. Theory*, vol. 54, pp. 2515–2534, Jun. 2008.

[5] U. M. Maurer, "Secret key agreement by public discussion from common information," *IEEE Trans. Inform. Theory*, vol. 39, pp. 733–742, May 1993.

[6] R. Ahlswede and I. Csiszár, "Common randomness in information theory and cryptography – Part I: Secret sharing," *IEEE Trans. Inform. Theory*, vol. 39, Jul. 1993.

[7] A. M. Sayeed and A. Perrig, "Secure wireless communications: Secret keys through multipath," *Proc. Int. Conf. Acoust. Speech, Signal Processing*, pp. 3013–3016, Mar. 2008.

[8] T. -H. Chou, A. M. Sayeed, and S. C. Draper, "Minimum energy per bit for secret key acquisition over multipath wireless channels," *Proc. Int. Symp. Inform. Theory*, pp. 2296–2300, Jun. 2009.

[9] T. -H. Chou, S. C. Draper, and A. M. Sayeed, "Key generation using external source excitation: Capacity, reliability and secrecy exponent," *IEEE Trans. Inform. Theory*, vol. 58, pp. 2455–2474, Apr. 2012.

[10] R. Wilson, D. Tse, R. A. Scholtz, and L. Fellow, "Channel identification: Secret sharing using reciprocity in UWB channels," *IEEE Trans. on Inform. Foren. and Sec*, pp. 364–375, Sep. 2007.

[11] C. Ye, A. Reznik, G. Sternberg, and Y. Shah, "On the secrecy capabilities of ITU channels," *Proc. Vehic. Tech. Soc. Conf.*, pp. 2030–2034, Oct. 2007.

[12] C. Ye, A. Reznik, and Y. Shah, "Extracting secrecy from jointly Gaussian random variables," *Proc. Int. Symp. Inform. Theory*, pp. 2593–2597, Jul. 2006.

[13] S. Nitinawarat, "Secret key generation for correlated Gaussian sources," *Proc. Int. Symp. Inform. Theory*, pp. 702–706, Jul. 2007.

[14] T. -H. Chou, A. M. Sayeed, and S. C. Draper, "Impact of channel sparsity and correlated eavesdropping on secret key generation from multipath channel randomness," *Proc. Int. Symp. Inform. Theory*, pp. 2518–2522, Jun. 2010.

[15] U. Maurer and S. Wolf, "Secret-key agreement over unauthenticated public channels – Part I: Definitions and a completeness result," *IEEE Trans. Inform. Theory*, vol. 49, pp. 822–831, Apr. 2003.

[16] U. Maurer and S. Wolf, "Secret-key agreement over unauthenticated public channels – Part II: The simulatability condition," *IEEE Trans. Inform. Theory*, vol. 49, pp. 832–838, Apr. 2003.

[17] U. Maurer and S. Wolf, "Secret-key agreement over unauthenticated public channels – Part III: Privacy amplification," *IEEE Trans. Inform. Theory*, vol. 49, pp. 839–851, Apr. 2003.

[18] T. -H. Chou, V. Y. F. Tan, and S. C. Draper, "The sender-excited secret key agreement model: Capacity and error exponents," *arXiv:1107.4148v2 [cs.IT]*, Dec. 2011.

[19] A. Agrawal, Z. Rezki, A. J. Khisti, and M. Alouini, "Non-coherent capacity of secret key agreement with public discussion," vol. 6, pp. 565–574, Sep. 2011.

[20] J. E. Hershey, A. A. Hassan, and R. Yarlagadda, "Unconventional cryptographic keying variable management," *IEEE Trans. Commun.*, vol. 43, pp. 3–6, Jan. 1995.

[21] A. A. Hassan, W. E. Stark, J. E. Hershey, and S. Chennakeshu, "Cryptographic key agreement for mobile radio," *Digital Signal Process.*, vol. 6, pp. 207–212, 1996.

[22] S. Mathur, W. Trappe, N. Mandayam, C. Ye, and A. Reznik, "Radiotelepathy: Extracting a secret key from an unauthenticated wireless channel," *ACM MobiCom*, pp. 128–139, Jun. 2008.

[23] C. Ye, S. Mathur, A. Reznik, Y. Shah, W. Trappe, and N. B. Mandayam, "Information-theoretically secret key generation for fading wireless channels," *IEEE Trans. Inform. Theory*, vol. 5, pp. 240–254, Jun. 2010.

[24] S. Jana, S. N. Premnath, M. Clark, and S. K. Kasera, "On the effectiveness of secret key extraction from wireless signal strength in real environments," *ACM MobiCom*, pp. 321–332, Sep. 2009.

[25] S. Mathur, R. Miller, A. Varshavsky, W. Trappe, and N. Mandayam, "Proximate: Proximity-based secure pairing using ambient wireless signals," *ACM MobiSys*, pp. 211–224, Jun. 2011.

[26] L. Xiao, L. Greenstein, N. Mandayam, and W. Trappe, "Fingerprints in the ether: Using the physical layer for wireless authentication," *Proc. Int. Conf. Commun.*, pp. 4646–4651, Jun. 2007.

[27] L. Xiao, L. Greenstein, N. Mandayam, and W. Trappe, "Using the physical layer for wireless authentication under time-variant channels," *IEEE Trans. Wireless Commun.*, vol. 7, pp. 2571–2579, Jul. 2008.

[28] S. Banerjee and A. Mishra, "Secure spaces: Location-based secure group communication for wireless networks," *ACM MobiCom*, vol. 7, pp. 68–70, Sep. 2002.

[29] J. W. Wallace and R. K. Sharma, "Automatic secret keys from reciprocal MIMO wireless channels: Measurement and analysis," *IEEE Trans. on Inform. Foren. and Sec*, vol. 5, pp. 381–392, Sep. 2010.

[30] J. Cardinal and G. V. Assche, "Construction of a shared secret key using continuous variables," *Proc. 2003 IEEE Infor. Theory Workshop (ITW2003)*, Mar. 2003.

[31] J. Cardinal, "Quantization with an information-theoretic distortion measure," tech. rep., Universit Libre de Bruxelles, 2002.

[32] S. Yasukawa, H. Iwai, and H. Sasaoka, "Adaptive key generation in secret key agreement scheme based on the channel characteristics in OFDM," *Proc. Int. Symp. Inform. Theory*, pp. 7–10, Dec. 2008.

[33] G. Brassard and L. Salvail, *Secret-key reconciliation by public discussion*, pp. 410–423. EUROCRYPT '93, Secaucus, NJ, USA: Springer-Verlag New York, Inc., 1994.

[34] M. Wilhelm, I. Martinovic, and J. B. Schmitt, "On key agreement in wireless sensor networks based on radio transmission properties," *Sec. Netwk. Protoc. Workshop*, pp. 37–42, Oct. 2009.

[35] A. M. Sayeed and T. Sivanadyan, "Wireless communication and sensing in multipath environments using multi-antenna transceivers," in *Handbook on Array Processing and Sensor Networks* (S. Haykin and K. J. R. Liu, eds.), ch. 5, Wiley, Apr. 2010.

[36] S. Wu and Y. Bar-Ness, "OFDM systems in the presence of phase noise: consequences and solutions," *IEEE Trans. Commun.*, vol. 52, pp. 1988–1996, Nov. 2004.

[37] IEEE 802.16 Workgroup, *RSSI mean and standard deviation*, ch. 8.3.9.2. IEEE Standards Association, 2009.

[38] A. Joarder, "Moments of the product and ratio of two correlated Chi-square variables," *Statistical Papers*, vol. 50, pp. 581–592, Mar. 2009.

[39] Y. Sutcu, S. Rane, J. S. Yedidia, S. Draper, and A. Vetro, "Feature extraction for a Slepian-Wolf biometric system using LDPC codes," *Proc. Int. Symp. Inform. Theory*, pp. 2297–2301, Jul. 2010.

[40] F. R. Kschischang, B. J. Frey, and H.-A. Loeliger, "Factor graphs and the sum-product algorithm," *IEEE Trans. Inform. Theory*, vol. 47, pp. 498–519, Feb. 2001.

[41] D. Slepian and J. K. Wolf, "Noiseless coding of correlated information sources," *IEEE Trans. Inform. Theory*, pp. 471–480, Jul. 1973.

[42] S. Wu and Y. Bar-Ness, "A phase noise suppression algorithm for OFDM-based WLANs," *IEEE Commun. Lett.*, vol. 6, pp. 535–537, Dec. 2002.

[43] IEEE Standards Association, "Wireless LAN Medium Access Control (MAC) and Physical Layer (PHY) Specifications," Jun. 2007.

[44] S. Verdu, "Spectral efficiency in the wideband regime," *IEEE Trans. Inform. Theory*, vol. 48, pp. 1319–1343, Jun. 2002.

[45] T. J. Richardson, M. A. Shokrollahi, and R. L. Urbanke, "Design of capacity-approaching irregular low-density parity-check codes," *IEEE Trans. Inform. Theory*, vol. 47, pp. 619–637, Feb. 2001.